Novel Wide Range Speed Control of Permanent Magnet Brushless Motor Drives

C.C. Chan, *Fellow, IEEE*, J.Z. Jiang, W. Xia, and *K.T. Chau, *Member, IEEE*

Department of Electrical and Electronic Engineering, University of Hong Kong, Hong Kong

* Department of Electrical Engineering, Hong Kong Polytechnic, Hong Kong.

Abstract - This paper presents a novel approach for wide range speed control of permanent magnet (PM) brushless motor drive, including both sinewave and squarewave versions. As compared with conventional flux-weakening control, the approach takes definite advantages that it can be applied to the squarewave PM brushless motor drive directly, and even to the motor drive with negligible mutual inductances between phase windings. Moreover, it is easier to implement than flux-weakening control because no coordinate transformation is needed. The key of this approach is to make use of the transformer EMF in such a way that it weakens the rotational EMF when the motor operates above the base speed, leading to achieve the constant power operation. Computer simulation and experimental results show that the proposed approach works well.

NOMENCLATURE

B	Damping constant.
E	Amplitude of rotational EMF.
e_j	Rotational EMF of phase j.
i_j	Current of phase j.
J	Moment of inertia.
L	Self-inductance of phase winding.
$L\frac{di_j}{dt}$	Transformer EMF of phase j.
R	Resistance of phase winding.
T_e	Electromagnetic torque.
T_l	Load torque.
v_j	Applied voltage of phase j.
V	Amplitude of applied voltage.
β	Lagging angle of phase current.
θ_0	Advanced conduction angle.
ω	Motor speed.

I. INTRODUCTION

With the advent of high energy permanent magnet (PM) materials, PM brushless motor drives are becoming more and more attractive for industrial applications and electric vehicles [1]-[3].As compared with induction motor drives, they possess some distinct advantages such as higher power density, higher efficiency, and better controllability.

PM brushless motor drives have sinewave and squarewave versions. The sinewave PM brushless motor drive, so-called the PM synchronous motor drive, is fed by sinewave current and uses continuous rotor position feedback signals to control the commutation. On the other hand, the squarewave PM brushless motor drive, so-called the PM brushless DC motor drive, is fed by squarewave current and uses discrete rotor position feedback signals to control the commutation. Since the interaction between squarewave current and squarewave magnetic field in the motor can produce a larger torque product than that produced by sinewave current and sinewave magnetic field, the PM brushless DC motor drive possesses higher power density than the PM synchronous motor drive [4], [5].

In most applications, particularly for electric vehicles, wide range speed control of motor drives is necessary. As shown in Fig. 1, when the motor speed is lower than the base speed, the motor drive is required to provide a constant output torque, so-called the constant torque operation. On the other hand, when the speed is higher than the base speed, the load torque decreases with the speed. Thus, instead of providing a constant output torque, the constant power operation is preferred because it can significantly reduce the cost and size of the motor drive.

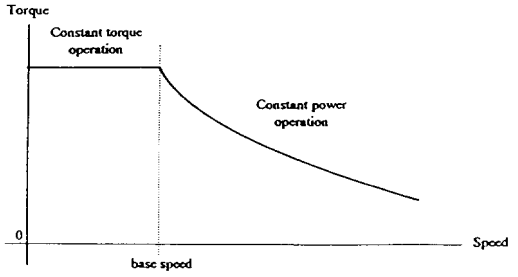

Fig. 1. Torque -speed envelope.

The constant torque operation can be easily achieved in any PM brushless motor drives [6]. However, when the speed is above the base speed, the rotational EMF increases rapidly so that the motor drive usually suffers from difficulty to achieve the constant power operation. Recently, flux-weakening control has been developed to deal with this problem. By employing the field component of stator current to weaken the airgap field produced by magnets, this approach allows some PM brushless motor drives to achieve the constant power operation [7], [8].

Although flux-weakening control has been accepted to be applicable to the PM synchronous motor drive, it can not

IEEE Catalogue No. 95TH8025
0-7803-2423-4/95/$4.00©1995 IEEE

readily be applied to the PM brushless DC motor drive. It is because the conventional *d-q* coordinate transformation, which is always used in the flux-weakening control algorithm, can not be directly applied to the squarewave motor drive. Although Fourier analysis can be employed to solve this problem by expressing the squarewave into the corresponding fundamental and harmonic sinewaves, it is too cumbersome to be realized. Moreover, when the motor is phase-decoupling such that the mutual inductances between phase windings are negligible, conventional flux-weakening control becomes ill-suited [9], [10].

It is the purpose of this paper to present a novel wide range speed control approach which allows all PM brushless motor drives to achieve the constant power operation when the motor speed is above the base speed. Moreover, since conventional flux-weakening control can not readily be applied to the PM brushless DC motor drive and is even inapplicable to the phase-decoupling motor drive, the presentation of the proposed approach is focused on a phase-decoupling PM brushless DC motor drive.

In Section II, the principle of operation of the proposed approach to the phase-decoupling PM brushless DC motor drive is described. The corresponding mathematical model is derived in Section III. Section IV is then devoted to describe the control system of the motor drive. Finally, computer simulation and experimental results are given in Section V.

II. PRINCIPLE OF OPERATION

Recently, a new type of polyphase multipole PM brushless DC motor has been developed [9], [10]. This motor possesses some distinct advantages of high power density, high efficiency, and excellent controllability. Because of the independence of flux paths inside the motor, the mutual inductances between phase windings are negligible. Thus, it is so-called the phase-decoupling motor. As shown in Fig. 2, a 5-phase 22-pole phase-decoupling PM brushless DC motor drive is used for exemplification

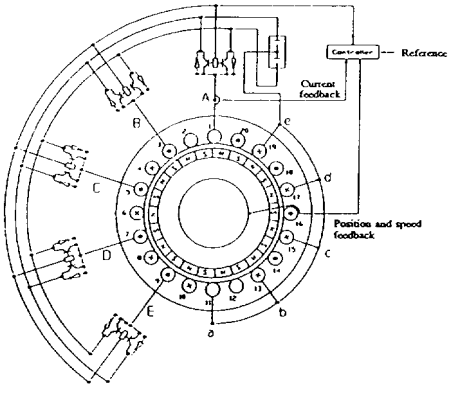

Fig. 2. Phase-decoupling PM brushless DC motor drive.

The basic concept of conventional flux-weakening control is to employ the field component of stator current to weaken the airgap field produced by magnets. Thus, the rotational EMF can be effectively reduced by making use of the mutual inductances between phase windings. However, because of phase-decoupling, it is impossible to apply this approach to this motor.

Fig. 3 illustrates the per-phase equivalent circuit diagram of the motor drive. During the constant torque operation, typical circuit waveforms are shown in Fig. 4. It can be found that the rotational EMF is generally lower than the applied voltage, and is in phase with the conduction period of T_1. When the motor speed is above the base speed, the rotational EMF becomes close to the applied voltage, resulting dramatic reduction in phase current and electromagnetic torque. In order to weaken the rotational EMF in the absence of mutual inductances, the transformer EMF is purposely employed to oppose the rotational EMF during the constant power operation. As shown in Fig. 5, the conduction period of T_1 leads the rotational EMF by a spatial angle, so-called the advanced conduction angle θ_0, when the motor speed is above the base speed.

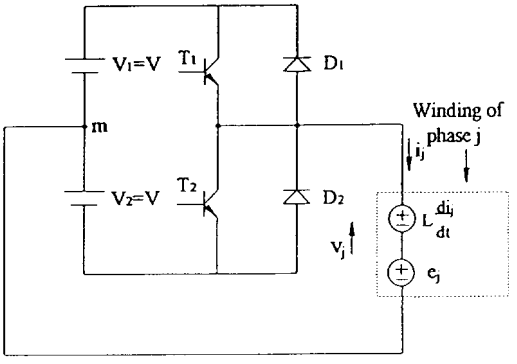

Fig. 3. Equivalent circuit diagram of phase *j*.

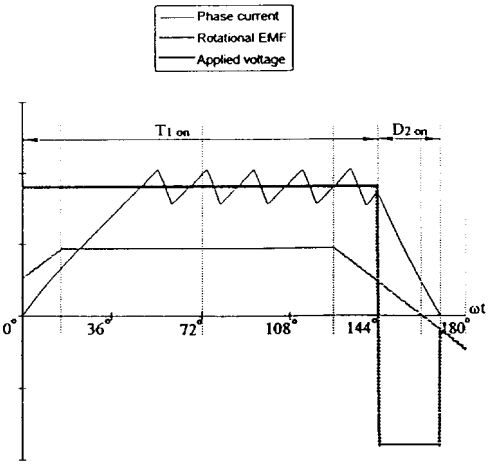

Fig. 4. Waveforms of constant torque operation.

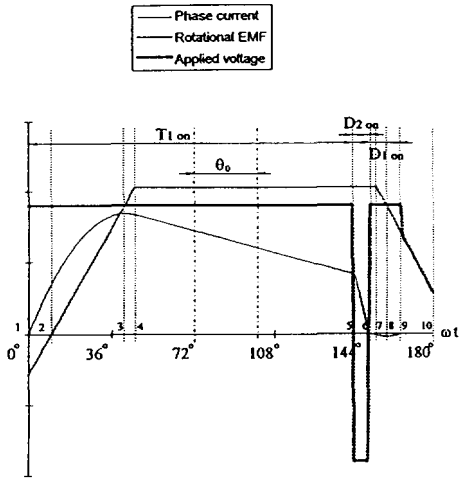

Fig. 5. Waveforms of constant power operation.

Starting from the turn-on of T_1, the first half cycle is divided into nine intervals as illustrated in Fig. 5. The operating principle is described in accordance with these intervals. In the interval 1-2, the negative rotational EMF acts to strengthen the applied voltage so that the phase current increases rapidly. In the interval 2-3, both the applied voltage and rotational EMF are positive. Since the applied voltage is still larger than the rotational EMF, the phase current increases gradually. Therefore, in both intervals, the transformer EMF is positive which indicates that energy is stored in the phase winding. On the other hand, in the intervals 3-4 and 4-5, the rotational EMF is greater than the applied voltage. Thus, the phase winding begins to release energy, and the phase current decreases gradually. Since the corresponding transformer EMF is negative, it acts to assist the applied voltage to counteract the rotational EMF. This phenomenon is the key point of this approach which is purposely employed to achieve the constant power operation. After T_1 is turned off, the phase current flows through D_2 in the interval 5-6. Since both the applied voltage and transformer EMF are negative, the phase current drops rapidly to zero. Then, in the intervals 6-7 and 7-8, the rotational EMF is larger than the applied voltage so that the phase current begins to flow negatively through D_1. When the rotational EMF becomes smaller than the applied voltage in the interval 8-9, the phase current goes back to zero. Since the circuit is opened in the interval 9-10, the applied voltage equals the rotational EMF. The operating principle for another half cycle is very similar and is omitted.

It should be noted that, to the best of the authors' knowledge, the use of transformer EMF to weaken the rotational EMF for obtaining the constant power operation has not been found in the literature of power electronics and drives.

III. MATHEMATICAL DERIVATION

Because of phase decoupling, the m-phase PM brushless DC motor can be treated as m separate DC motors. Since the magnets, which are mounted on the rotor surface, possess low permeability, the induced current inside the rotor is negligible. Due to the symmetry of the motor configuration, the self inductances of phase windings are assumed to be identical. Thus, the voltage equation for the j-th phase of the motor can be expressed as

$$v_j(\omega t+\theta_o-\frac{(j-1)\pi}{m}) = R\,i_j(\omega t+\theta_o-\frac{(j-1)\pi}{m}) + L\frac{di_j(\omega t+\theta_o-\frac{(j-1)\pi}{m})}{dt} + e_j(\omega t-\frac{(j-1)\pi}{m}) \quad j=1\cdots m \tag{1}$$

On the other hand, the electromagnetic torque and the corresponding equation of motion are given by

$$T_e(\omega t) = \sum_{j=1}^{m} e_j(\omega t-\frac{(j-1)\pi}{m})\; i_j(\omega t+\theta_o-\frac{(j-1)\pi}{m})/\omega \tag{2}$$

$$T_e(\omega t)-T_l-B\omega(t)=J\frac{d\omega(t)}{dt} \tag{3}$$

Equations (1) and (3) can be rewritten as

$$i_j(\omega t+\theta_o-\frac{(j-1)\pi}{m}) = \frac{1}{L}\int_0^t[v_j(\omega t+\theta_o-\frac{(j-1)\pi}{m})-e_j(\omega t-\frac{(j-1)\pi}{m}) - R\,i_j(\omega t+\theta_o-\frac{(j-1)\pi}{m})]dt+i_j(0) \tag{4}$$

$$\omega(t)=\frac{1}{J}\int_0^t[T_e(\omega t)-T_l-B\,\omega(t)]dt\;\;\omega(0) \tag{5}$$

where $i_j(0)$ and $\omega(0)$ are the corresponding initial values. Since the motor possesses a unique configuration, the self inductance is obtained using finite element method [9].

In order to obtain the analytical solution of (4), a piecewise continuous function is used to represent the phase current. For simplicity, the following assumptions are made:

i) The phase winding resistance is negligible.
ii) The induced rotational EMF is trapezoidal.
iii) The initial spatial angle of phase current is zero, $\theta_o-\frac{(j-1)\pi}{m}=0$.
iv) The initial phase current is zero, $i_j(0)=0$.

Starting from the moment that T_1 is turned on, the phase current can be divided into six stages over the first half cycle as shown in Fig. 5.

A. Stage I, $[\theta_o+\frac{\pi}{2m}\geq\omega t\geq 0]$

This stage covers the intervals 1-2, 2-3 and 3-4. The applied voltage is kept constant while the rotational EMF rises up linearly, which are given by

$$\left.\begin{aligned} v_j &= V \\ e_j &= \frac{mE\omega}{\pi}\left(t-\frac{\theta_o}{\omega}+\frac{\pi}{2m\omega}\right) \end{aligned}\right\} \quad (6)$$

Substituting (6) into (4) and using the zero initial condition, $i_j(0)=i_{j,1}=0$, the phase current can be obtained as

$$i_j(\omega t)=\frac{2V\pi-E\pi+2mE\theta_o}{2\pi\omega L}\omega t-\frac{mE}{2\pi\omega L}(\omega t)^2 \quad (7)$$

This stage finishes when $\omega t=\theta_o+\frac{\pi}{2m}$, the corresponding phase current is expressed as

$$i_{j,4}=\frac{\pi+2m\theta_o}{2m\omega L}V+\frac{4m^2\theta_o{}^2-4m\pi\theta_o-3\pi^2}{8m\pi\omega L}E \quad (8)$$

B. Stage II, $[\frac{m-1}{m}\pi \geq \omega t \geq \theta_o+\frac{\pi}{2m}]$

It covers the interval 4-5 in which both the applied voltage and rotational EMF are constant. They are given by

$$\left.\begin{aligned} v_j &= V \\ e_j &= E \end{aligned}\right\} \quad (9)$$

Substituting (9) into (4) and using $i_j(0)=i_{j,4}$, it yields

$$i_j(\omega t)=\frac{1}{\omega L}(V-E)(\omega t-\theta_o-\frac{\pi}{2m})+i_{j,4} \quad (10)$$

At the end of this stage, the phase current is given by

$$i_{j,5}=\frac{1}{\omega L}(V-E)(\pi-\theta_o-\frac{3\pi}{2m})+i_{j,4} \quad (11)$$

C. Stage III, $[\frac{m-1}{m}\pi+\beta \geq \omega t \geq \frac{m-1}{m}\pi]$ It covers the interval 5-6, and its duration is defined as β. At the beginning of this stage, T_1 is turned off. Thus, D_2 is forward biased and begins to conduct the phase current. The applied voltage becomes negative while the rotational EMF is unchanged. They are given by

$$\left.\begin{aligned} v_j &= -V \\ e_j &= E \end{aligned}\right\} \quad (12)$$

Substituting (12) into (4) and using $i_j(0)=i_{j,5}$, the phase current is expressed as

$$i_j(\omega t)=-\frac{1}{\omega L}(V+E)(\omega t-\frac{m-1}{m}\pi)+i_{j,5} \quad (13)$$

At the end of this stage, the phase current is given by

$$i_{j,6}=-\frac{1}{\omega L}(V+E)\beta+i_{j,5} \quad (14)$$

which is equal to zero. Hence, by using (14), the duration of this stage can be found as

$$\beta=\frac{\omega L}{V+E}i_{j,5} \quad (15)$$

which is so-called the lagging angle of phase current.

D. Stage IV, $[\frac{2m-3}{2m}\pi+\theta_o \geq \omega t \geq \frac{m-1}{m}\pi+\beta]$

This stage covers the interval 6-7. Since the rotational EMF is larger than the applied voltage, D_1 is forward biased and begins to conduct the phase current negatively. Both the applied voltage and rotational EMF are kept constant, which are given by

$$\left.\begin{aligned} v_j &= V \\ e_j &= E \end{aligned}\right\} \quad (16)$$

Substituting (16) into (4) and using the zero initial condition, the phase current is expressed as

$$i_j(\omega t)=\frac{1}{\omega L}(V-E)(\omega t-\frac{m-1}{m}\pi-\beta) \quad (17)$$

At the end of this stage, it is given by

$$i_{j,7}=\frac{1}{\omega L}(V-E)(\theta_o-\beta-\frac{\pi}{2m}) \quad (18)$$

E. Stage V, $[\frac{2m-3}{2m}\pi+\theta_o+\gamma \geq \omega t \geq \frac{2m-3}{2m}\pi+\theta_o]$

It covers the intervals 7-8 and 8-9, and its duration is defined as γ. The applied voltage is kept constant while the rotational EMF decreases linearly. They are given by

$$\left.\begin{aligned} v_j &= V \\ e_j &= -\frac{mE\omega}{\pi}\left(t-\frac{\pi}{\omega}-\frac{\theta_o}{\omega}+\frac{\pi}{2m\omega}\right) \end{aligned}\right\} \quad (19)$$

Substituting (19) into (4) and using $i_j(0)=i_{j,7}$, it yields

$$\begin{aligned} i_j(\omega t) &= \frac{1}{\omega L}(V-mE+\frac{E}{2}-\frac{m\theta_o E}{\pi})(\omega t-\frac{2m-3}{2m}\pi-\theta_o) \quad (20) \\ &+\frac{mE}{2\pi\omega L}[(\omega t)^2-(\frac{2m-3}{2m}\pi+\theta_o)^2]+i_{j,7} \end{aligned}$$

The phase current at the end of this stage is given by

$$i_{j,9}=\frac{mE}{2\pi\omega L}\gamma^2+\frac{V-E}{\omega L}\gamma+i_{j,7} \quad (21)$$

Since the rotational EMF falls below the applied voltage in the interval 8-9, the phase current goes back to zero at the end of this stage. Hence, the duration of this stage can be easily obtained from (21).

F. Stage VI, $[\pi \geq \omega t \geq \frac{2m-3}{2m}\pi+\theta_o+\gamma]$

This stage covers the interval 9-10 and finishes at the end of the first half cycle. Since the circuit is opened, the applied voltage equals the rotational EMF while the phase current is always zero.

Since $i_j(\omega t+\pi)=-i_j(\omega t)$, the analytical formulae of phase current for another half cycle can readily be obtained. It should be noted that although the above derivation is based on the typical situation that $\frac{3\pi}{2m} \geq \theta_o \geq \frac{\pi}{2m}+\beta$, the derivation for other situations can be obtained similarly.

IV. CONTROL SYSTEM

Fig. 6 illustrates the closed-loop control system of the motor drive, which are suitable for both the constant-torque operation and constant power operation. When the speed reference signal ω^* is set, the motor starts up. According to the output of encoder (E), the speed feedback (SF) and position feedback (PF) produce the speed feedback signal ω and position feedback signal θ, respectively. The difference between speed reference and feedback signals is inputted

into the speed regulator (SR) in which proportional-integral control is adopted. According to the value of speed feedback signal, the operation indicator (OI) determines which mode of operation is required. The output signals from SR and OI are combined through a multiplier (X) to generate the torque reference T^*. Based on the output signal from OI, the angle generator (AG) provides the advanced conduction angle θ_0 which is zero during the constant torque operation, and non-zero during the constant power operation. The current feedback (CF) measures the stator phase current and produces the current feedback signal i. Feeding all reference and feedback signals into the logic signal generator (LSG), the corresponding output signal is used to drive the logic circuit (LC) for the power switching devices.

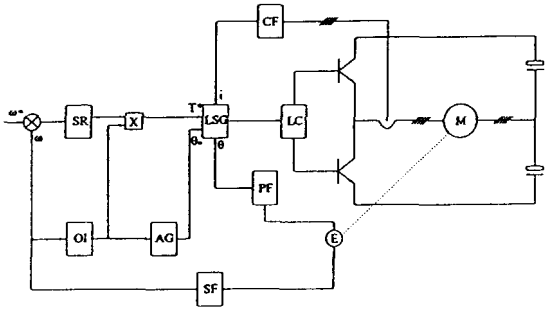

Fig. 6. Block diagram of control system.

It should be noted that the advanced conduction angle can be used as a controlled parameter for pursuing some specific performances. For example, the use of it for efficiency optimising control over the whole operating range is under investigation. In this paper, the effectiveness of using the advanced conduction angle to allow for the constant power operation is particularly focused.

V. RESULTS

The technical data of the motor are listed in Appendix. By using the formulae derived in Section III, computer simulation can readily be carried out. When the motor speed is 2747 rpm and the advanced conduction angle is 28°, the simulated phase current waveform is shown in Fig. 7, Under the same conditions, the measured phase current waveform is shown in Fig. 8. It can be found that they are very similar. Furthermore, a wide range speed control test is carried out up to 2.75 times the base speed in which there is no advanced angle during the constant torque operation while the advanced angle is fixed at 28° during the constant power operation. As shown in Fig. 9, the corresponding theoretical and experimental torque-speed envelopes are plotted together in which the agreement is good.

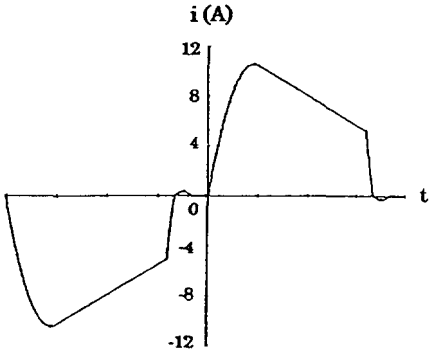

Fig. 7. Theoretical phase current waveform (4 A/div, 250 μs/div).

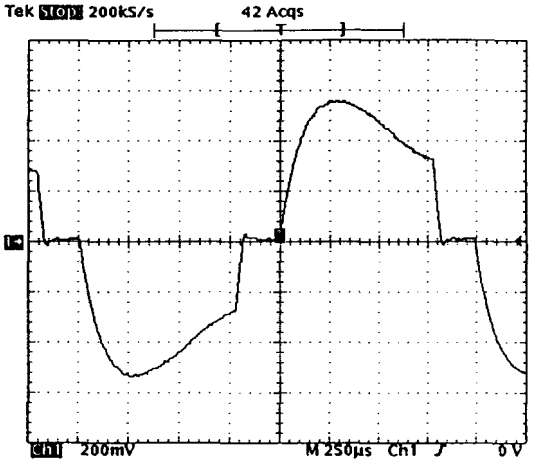

Fig. 8. Experimental phase current waveform (4 A/div, 250 μs/div).

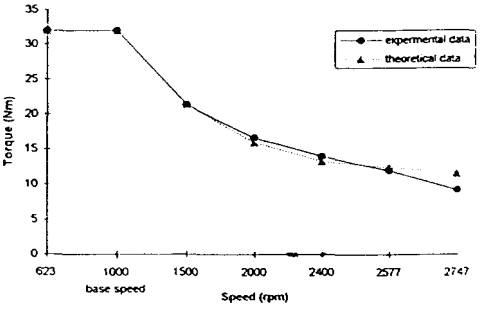

Fig. 9. Theoretical and experimental torque-speed envelopes.

VI. CONCLUSION

A novel wide range speed control approach is presented. It is suitable for all PM brushless motor drives, including the PM synchronous motor drive and PM brushless DC motor drive. The approach takes definite advantages over conventional flux-weakening control - it can be directly applied to the PM brushless DC motor drive; it can be applied to any brushless motor drives with negligible mutual inductances between phase windings; and it can be implemented without coordinate transformation. The originality of this approach is to make use of the transformer EMF in such a way that it weakens the rotational EMF when the motor operates above the base speed, leading to achieve the constant power operation. A 5-phase 22-pole phase-decoupling PM brushless DC motor drive is used for exemplification, and operates up to 2.75 times the base speed. Both computer simulation and experimental verification show that the proposed approach works well.

APPENDIX

Technical data of the motor

Rated power	3.33 kW
Rated voltage	2×90 V
Base speed	1000 rpm
No. of phase	5
Stator	
No. of slots	20
Outer diameter	175 mm
Inner diameter	86 mm
Length of core	100 mm
Winding type	Single layer
No. of coils	10
Resistance per phase (75°)	0.054Ω
Self-inductance per phase	1.29 mH
Slot pitch	1 slot
Rotor	
No. of poles	22
Outer diameter	84 mm
Inner diameter	48 mm
Magnet height	5 mm
Magnet material	Nd-Fe-B

REFERENCES

[1] T.J.E. Miller, *Brushless Permanent-Magnet and Reluctance Motor Drives.* Oxford University Press, New York, 1989.

[2] B.K. Bose, "A high-performance inverter-fed drive system of an interior permanent magnet synchronous machine," *IEEE Transactions on Industry Applications,* vol. IA-24, pp. 987-997, Nov./Dec. 1988.

[3] C.C. Chan, "Overview of electric vehicle technology," *IEEE Proceedings,* vol. 81, pp. 1202-1213, Sept. 1993.

[4] H. Weh, H. Mosebach, and H. May, "Design concepts and force generation in inverter-fed synchronous machines with permanent magnet excitation," *IEEE Transactions on Magnetics,* vol. 20, pp. 1756-1761, 1984.

[5] P.J. McCleer, J. M. Bailey, J. S. Lawler, and B. Banerjee, "Five phase trapezoidal back emf PM synchronous machines and drives," in *Proceedings European Power Electronics Conference*, Florence, Italy, 1991.

[6] K.T. Chau, *Computer Graphics Aided Design and Microcomputer Control of an Advanced Permanent Magnet Motor Drive*. MPhil Thesis, University of Hong Kong, 1990.

[7] B. Sneyers, D.W. Novotny, and T.A. Lipo, "Field weakening in buried permanent magnet AC motor drives," *IEEE Transactions on Industry. Applications,* vol. IA-21, pp. 398-407, Mar./Apr. 1985.

[8] T.M. Jahns, "Flux-weakening regime operation of an interior permanent-magnet synchronous motor drive," *IEEE Transactions on Industry Applications,* vol. IA-23, pp. 681-689, July/Aug. 1987.

[9] C.C. Chan, J.Z. Jiang, G.H. Chen, and X.Y. Wang, "A novel high power density permanent magnet variable-speed motor," *IEEE Transactions on Energy Conversion,* vol. 8, pp. 297-303, June 1993.

[10] C.C. Chan, "A novel permanent magnet brushless DC motor," UK Patent Application, 1994.